Collective optical Thomson scattering in pulsed-power driven high energy density physics experiments (invited)

L. G. Suttle,[1,a)] J. D. Hare,[1] J. W. D. Halliday[1], S. Merlini[1], D. R. Russell[1], E. R. Tubman[1], V. Valenzuela-Villaseca[1], W. Rozmus[2], C. Bruulsema[2] and S. V. Lebedev[1]

[1]Blackett Laboratory, Imperial College, London, SW7 2BW, United Kingdom
[2]Theoretical Physics Institute, University of Alberta, Edmonton, Alberta T6G 2J1, Canada

Optical collective Thomson scattering is used to diagnose magnetized high energy density physics experiments at the Magpie pulsed-power generator at Imperial College London. The system uses an amplified pulse from the 2nd harmonic of a Nd:YAG laser (3 J, 8 ns, 532 nm) to probe a wide diversity of high-temperature plasma objects; with densities in the range of 10^{17}-10^{19} cm^{-3} and temperatures between 10 eV and a few keV. The scattered light is collected from 100 μm-scale volumes within the plasmas, which are imaged onto optical fiber arrays. Multiple collection systems observe these volumes from different directions, providing simultaneous probing with different scattering K-vectors (and different associated α-parameters, typically in the range $0.5 - 3$) allowing independent measurements of separate velocity components of the bulk plasma flow. The fiber arrays are coupled to an imaging spectrometer with a gated ICCD. The spectrometer is configured to view the ion-acoustic waves (IAWs) of the collective Thomson scattered spectrum. Fits to the spectra with the theoretical spectral density function $S(K,\omega)$ yield measurements of the local plasma temperatures and velocities. Fitting is constrained by independent measurements of the electron density from laser interferometry, and the corresponding spectra for different scattering vectors. This TS diagnostic has been successfully implemented on a wide range of experiments, revealing temperature and flow velocity transitions across magnetized shocks, inside rotating plasma jets and imploding wire arrays, as well as providing direct measurements of drift velocities inside a magnetic reconnection current sheet.

I. INTRODUCTION

Thomson scattering (TS) is a powerful diagnostic tool in high energy density physics (HEDP) experiments, as it allows local time-resolved measurements of key plasma parameters. By contrast, most other methods for probing HEDP plasmas either provide measurements which are complicated by spatial integration along a probe path (e.g. interferometry, shadowgraphy, radiography) or are highly perturbative (e.g. inductive probes). Due to the detailed and quantitative nature of TS measurements, it is possible to gain insights into acceleration, heating and energy-exchange mechanisms in systems with complex structures and steep density gradients, which evolve on nano-second timescales.

At the Magpie pulsed-power generator[1], TS is used to diagnose HEDP experiments[2,3] studying the interactions of supersonic flows of magnetized, high-temperature and high-atomic number plasmas (average ionization $\bar{Z} \gg 1$). The plasma flows are produced inside a vacuum chamber, by the application of a 500 ns, 1.4 MA-peak current pulse to a load of either thin metal wires or foils, which creates an ablated plasma that is accelerated by the global $J \times B$ force. The plasma flows are continuous throughout the current-drive and have centimeter length scales, with dynamic timescales in the range 5-100 ns and flow velocities of the order of 100 km/s, corresponding to sonic Mach numbers of ≤ 5. The electron densities in these plasmas typically range between

10^{17}-10^{19} cm^{-3} and are accompanied by embedded magnetic fields of several Tesla (originating from the drive current), which are advected with the flows.

The interactions of these flows with either stationary obstacles or counter-propagating flows generate shock structures, with associated plasma heating (reaching temperatures between 10 eV and several keV) and in some cases reconnection of the embedded magnetic fields. To investigate the fundamental plasma physics processes occurring in these scenarios, a TS diagnostic is employed to track how the temperatures and flow velocities of the plasma flows evolve across the interaction regions.

In this paper we provide a detailed description of the specification and implementation of the optical TS system used to diagnose the experiments carried out on the Magpie generator (section II). We also demonstrate the capabilities of the diagnostic with specific examples of data obtained from a variety of experimental applications (section III).

II. EXPERIMENTAL IMPLEMENTATION

A. Overview of the diagnostic system

TS systems used in HEDP experiments typically provide measurements with continuous temporal resolution at a single location by imaging TS light onto a streaked spectrometer[4–13]. Alternative setups provide continuous spatial resolution by imaging an extended scattering region
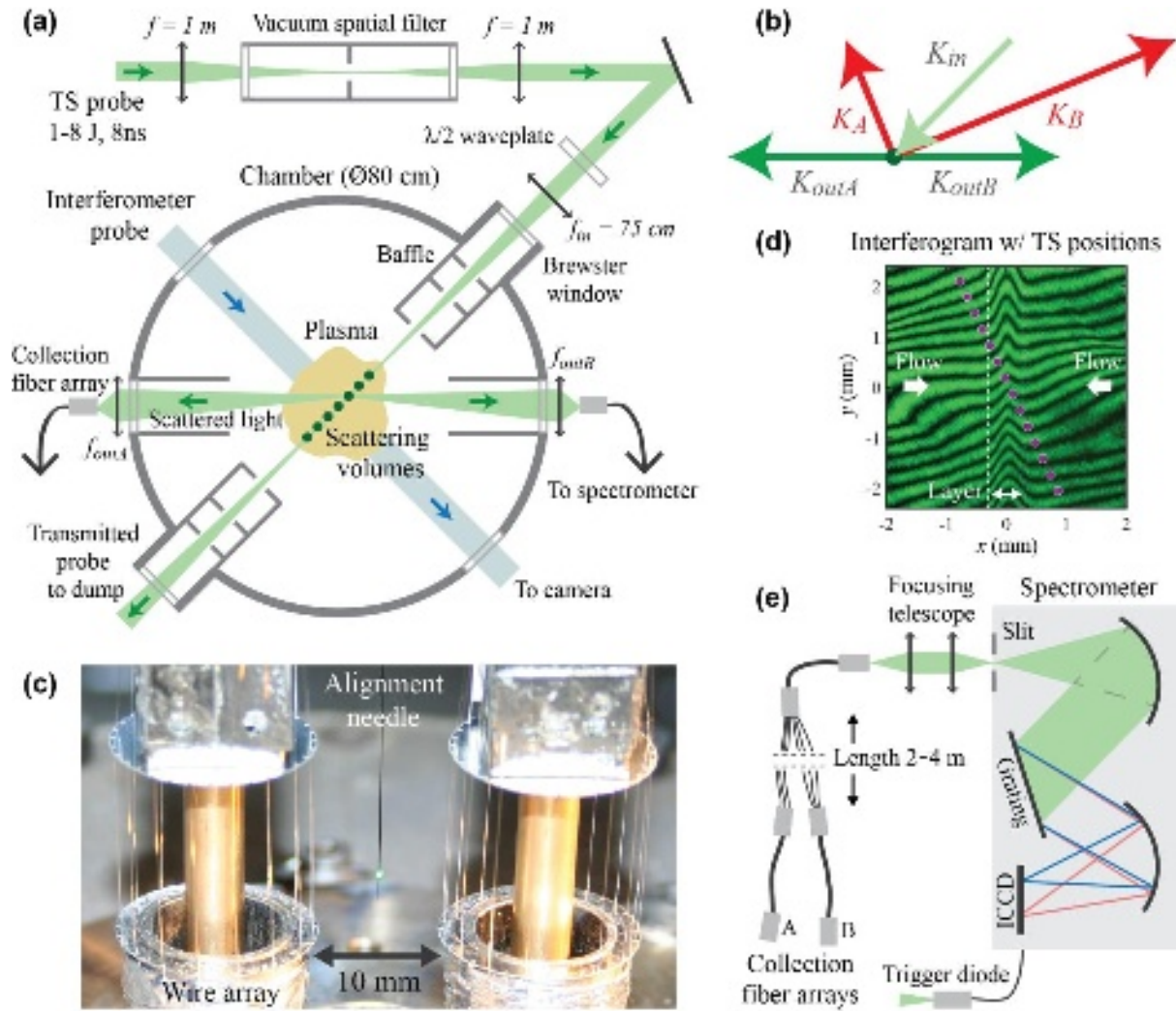
a) Email: l.suttle10@imperial.ac.uk

FIG. 1. (a) Schematic top-down view of the Magpie experiment chamber (not to scale), showing the key components and optical path of the TS system for an example probe-scattering geometry. (b) Probe (K_{in}), collection (K_{out}) and scattering (K) vectors corresponding to the TS geometry in (a). (c) Image of the probe laser incident on an alignment needle positioned between two wire arrays. (d) $\varnothing 125\,\mu m$ TS volumes (red dots, to scale) overlaid on an interferogram from a reconnection experiment. (e) Schematic diagram showing the coupling of the fiber bundles to the imaging spectrometer.

onto the input slit of a time-gated spectrometer[14–16]. Despite numerous strengths, the adaptability of such systems can be limited by physical and time restrictions of repositioning the spectrometer and delivery optics to adjust the scattering locations and angles. The Magpie TS diagnostic provides time-gated measurements from multiple discrete locations and aims to offer increased versatility and reconfigurability of the scattering geometry by employing optical fiber relay of TS light to the spectrometer. The diagnostic consists of: (1) a high-power laser which probes along narrow chord through the region of interest of the plasma, (2) arrays of optical fibers which collect the light scattered from multiple positions along the probe path, and (3) a time-gated imaging spectrometer which records the spectrum collected by each fiber.

The diagnostic utilizes optical TS in the collective regime, where light is scattered from the coherent fluctuations of shielding electron clouds in the plasma ($\alpha \equiv 1/K\lambda_D \gtrsim 1$, where λ_D is the Debye length of the plasma)[17]. The spectrometer is configured to view the ion acoustic waves (IAWs) of the TS spectra. Fits of the IAWs with the spectral density function $S(K,\omega)$ provide measurements of: the product of average ionization and electron temperature ($\bar{Z}T_e$), the ion temperature (T_i), the bulk flow velocity (V_{flow}) and, in the presence of currents, the relative drift velocity between ions and electrons (U_{drift}); where all velocity measurements are in the direction of the scattering vector K[17].

Figure 1(a) shows a schematic diagram of the optical path of the TS diagnostic through the Magpie experiment chamber for a typical scattering geometry. The cylindrical

chamber ($\emptyset$~80 cm) has 16 equally spaced radial ports (separated by 22.5°), and a vertical (out of page) port, which nominally define the available probing and scattering directions. In the experimental setup careful choice is made of the probe and collection directions ($\widehat{K}_{in}$ and $\widehat{K}_{out}$ respectively), to select the most appropriate direction of K ($= K_{out} - K_{in}$) for the velocity component of interest, as well as to optimize sensitivity to the temperature parameters through the magnitude of K – which affects both the spectral resolution by broadening of the spectra ($\delta\omega = K \cdot V$) and the TS regime by adjustment of the α-parameter[17]. For the typical parameters obtained in our experiments, α-values lie in the range $0.5 - 3$[18–24].

Multiple fiber-optic collection systems are deployed to simultaneously view scattered light from the same or overlapping locations, with different K (this is illustrated in Figure 1(a), with the geometry of the corresponding vectors in Figure 1(b)). This allows independent measurement of the separate velocity components of the plasma along the directions of the K-vectors, as well as co-constraint of the temperature parameters[25], or checks for temperature anisotropy.

To further constrain the parameters of the spectral fits, laser interferometry is used to make independent measurements of the electron density of the plasma[26–29]. This allows the electron density to be treated as a known parameter, thus reducing the free parameters of the fits.

B. Probe laser

The laser probe is seeded by a standard Q-switched Nd:YAG laser (Spectra-Physics Quanta-Ray GCR-230: 1064 nm, $\Delta\lambda$=0.34 pm, 5 Hz, ≤1 J). A single pulse of 160 mJ is amplified on a double pass through a Nd:Silicate rod amplifier (25 mm diameter, 400 mm length) resulting in up to 20 J at 1064 nm (10±1 J in standard operation). This is frequency doubled to the 2nd harmonic by a 4 cm long type 2 KDP crystal, producing a linearly-polarized 532 nm, 8 ns-FWHM pulse of typically 2-4 J on target. This laser energy is sufficient to produce scattered light in the target plasma with a strong signal-to-noise ratio (typically ~10-50) of the IAW feature relative to the intense, broadband self-emission of the plasma; whilst remaining non-perturbative (in terms of heating by inverse bremsstrahlung[30–33]) for the majority of our experimental applications. The 532 nm wavelength of the probe is both practical for visual alignment, and places the diagnostic in the collective regime for a wide range of experimental conditions and viewing angles.

After amplification, the laser beam travels a further distance of ~20 m to the experiment chamber in order to accommodate a suitable time-of-flight delay to trigger the spectrometer (see section IID). Prior to delivery into the chamber, the probe beam is apodized and spatially filtered inside a vacuum relay tube (Figure 1(a)) in order to provide a clean Gaussian beam profile and remove any higher order modes. This minimizes the presence of any beam "halo" which could potentially produce reflected stray light, as the

beam is often required to pass close to the surfaces of the experimental hardware (electrodes, wires, etc.) inside the chamber. The suppression of stray light in these experiments is a critical consideration, as the unwanted signal is superimposed on the TS scattered spectra if it is picked up by the collection optics. This can result in spectra that are either fully or partially obscured in the region of the unshifted laser wavelength, which introduces an additional fitting parameter for the spectra, and thus reduces the confidence of the fitted plasma parameters.

On injection to the chamber, the collimated probe beam ($\emptyset$25 mm) is focused using an anti-reflection (AR) coated, $\emptyset$2" plano-convex lens with focal length f_{in} =75 cm (Thorlabs LA1727). For a perfect Gaussian beam profile, this would be expected to produce a diffraction-limited beam waist of $w_0 =$ 20 μm, with a Rayleigh length of $z_R = 2.5$ mm[34]. However, due to imperfections in the beam profile, the actual focal spot size is approximately an order of magnitude larger. By moving a beam block transverse to the beam around the focal position, we estimate an effective beam waist of ≤250±50 μm over a range of ±10 mm from the focus. Thus, this can be treated as the upper limit of the transverse spatial scale of scattering volumes within the plasma.

On entry to the experiment chamber, the probe beam passes through a window positioned at the Brewster angle. The window is orientated such that the axis of the transmitted (p-polarized) light is orthogonal to the plane of the collection optics, as this maximizes the scattered signal intensity within the collection plane[17]. Upstream of the Brewster window, a half-wave plate is used to match the linear polarization of the beam to the window, to minimize reflective loses at the interface which could reduce signal intensity and contribute to stray light. At the far-side of the chamber the transmitted fraction of the probe beam exits via a co-aligned Brewster plate, and is dumped far from the region of experimental interest – again to minimize stray light. Inside the chamber, the path of the probe is baffled both up and downstream of the scattering region, to reduce the likelihood of stray reflections reaching the collection optics.

C. Collection optics and alignment procedure

The collection optics image the path of the probe beam through the plasma onto a linear array of optical fibers, where each fiber defines a separate scattering volume along the path (Figure 1(a)). In the majority of experiments, multiple collection systems are deployed, each with their own imaging lenses and fiber array. These generally view the same or overlapping scattering volumes from different directions, providing simultaneous TS measurements with different scattering K-vectors.

The imaging optics typically comprise of a single AR coated, $\emptyset$2" achromatic lens (Thorlabs AC508 series, $f = 15$ $– 25$ cm), placed directly outside of the chamber viewport windows (at a distance of ~43 cm from the scattering volumes) to protect the optics from plasma debris. This provides an acceptance half-angle for the scattered light of

Table I. Inventory of fiber arrays.

Fiber diameter (μm)	# of fibers	Spacing (μm)	Array length (mm)	Inventory
100	7	250	1.50	6
100	14	250	3.25	2
100	22	250	5.25	1
100	28	250	6.75	1
100	44	125	5.38	1
100	44	250	10.75	1
200	7	390	2.34	2
200	14	390	5.07	1

3° and a magnification of the scattering volumes of 0.5 – 1.4. However, in situations where the intensity of the TS signal is limited, a two-lens collection telescope is placed inside the experiment chamber at a distance of ~15 – 20 cm, increasing the acceptance half-angle to ~7 – 9°. This wider aperture collects more light but results in a greater range of K-vectors being sampled by the measurement, which needs to be considered when fitting the spectra and extracting velocity measurements (see section IIE). To limit the collection of stray light from spurious reflections, the fields of view of the collection lenses are restricted by baffles inside the experiment chamber.

The optical fiber arrays (custom built by LEONI) used to collect the scattered light are composed of equally spaced fibers arranged in a line. Our inventory of arrays (listed in Table I) provides several options for the size, spacing and number of the fibers. The combination of the size of the fibers and the magnification of the imaging system defines the areal size of the scattering volumes. In the majority of experiments to date (including those presented in section III) arrays of 14 fibers of Ø100 μm diameter were used. The fibers in these arrays are spaced by "dead-fibers" creating a center-to-center distance of 250 μm between the active fibers. However, recent additions to the inventory include an array of 44 adjacent (active) fibers, which allows a more continuous sampling of the plasma parameters, and 6 arrays of $7 \times$ Ø100 μm fibers to increase the number of possible simultaneous scattering angles in a single experiment. In all cases the acceptance half-angle of the fibers is 12.7°, which utilizes the full collection by the lenses.

To align the fiber arrays to the scattering positions, a thin metal needle (Ø200 μm) is inserted into the probe path (Figure 1(c)) using a micrometer-precision, 3D Cartesian translation stage. The stage operates under vacuum to prevent misalignment during pump-down, and it is configured to allow independent translation of the needle parallel and perpendicular to the beam in the collection plane, with 25 mm orthogonal ranges providing full access to the range of scattering volumes. The stage also facilitates motion in the vertical direction (out-of-page in Figure 1(a)), with a range of 50 mm, so that the needle can be removed after alignment. During alignment, the needle is centered on the probe beam by observing the diffraction pattern in the transmitted light at the exit port. The shaft of the needle is

generally orientated such that the light scattered by the probe laser forms a ring in the collection plane, passing through the center of the collection lenses. This provides a well-defined focal point to check in turn the positioning and focus of each fiber.

To determine the coordinates of the scattering volumes with respect to the overall plasma structure, the light scattered by the alignment needle is also imaged onto the cameras of the laser interferometry diagnostic[26–29]. The interferometry diagnostic utilizes a separate Q-switched Nd:YAG laser at the 2nd harmonic (EKSPLA SL312P: 532 nm, 0.3 ns, 200 mJ) to probe the plasma. The diagnostic typically consists of two simultaneous Mach-Zehnder interferometers: one probing along a radial direction of the chamber (as shown in Figure 1(a)), and one along the vertical axis of the chamber (into the page in Figure 1(a)). The interferograms are recorded on DSLR cameras (Canon 500D) with external, AR-coated imaging lenses (Thorlabs Ø3" achromats or Ø4" singlets). The interferometer cameras are focused on the plane of the TS measurements, providing a field of view of around Ø25 mm. Background images are recorded on each camera of the scatter of the TS probe from the alignment needle at each of the scattering volume locations. The orthogonal images allow the full Cartesian coordinates of the volumes to be constructed.

To identify the electron density of the plasma at each scattering volume, the background images are overlaid with the interferograms from the experiment, and the positions of the volumes are marked (Figure 1(d)). The interferograms display interference patterns whose fringes are locally phase-shifted (with respect to background images) by an amount proportional to the integrated electron density along the probing direction ($\Delta\phi \propto \int n_e dl$). The interferograms are processed to interpolate the phase shift (and hence integrated electron density) at each position in the image[26–28]. By design, the plasma structure often displays uniformity along at least one of the probing directions (which can be confirmed from the orthogonal viewing direction), and so the integrated electron densities can be divided by the probing length L to extract estimates of the local electron density at each scattering volume.

D. Spectrometer coupling

The light collected by the fiber arrays is coupled to a Czerny-Turner imaging spectrometer (Andor Shamrock 500i) as shown in Figure 1(e). The multiple fiber arrays are joined to a single array by high-precision SMA fiber connectors (Thorlabs ADASMA). The light is then coupled from the fiber array to the spectrometer entrance slit with a 1:1 telescope (Thorlabs MAP107575, $f_1 = f_2 = 75$ mm) which images the individual fiber outputs onto the slit to maximize the transmitted signal.

To view IAWs of the TS spectra the spectrometer uses a grating of 2400 lines/mm, giving a range of ± 7 nm from the central laser wavelength (λ_0), which is ample for the expected feature widths ($\sim 1 - 4$ Å) and Doppler shifts in our experiments ($\Delta\lambda \sim 2$Å for $V_{flow} \sim 100$ km/s). This grating is typically used in combination with a 20 μm slit width, yielding a spectral resolution of 0.25 Å, which provides sufficient detail to fit the IAW spectra of mid-Z elements such as aluminum from $\bar{Z}T_e \gtrsim 5$ eV, or high-Z elements such as tungsten from $\bar{Z}T_e \gtrsim 13$ eV.

The spectrometer records the TS spectra on a time-gated, intensified charge coupled device (ICCD) camera (Andor iStar 740: 512×2048 pixels). The ICCD time gate is triggered by a photodiode placed ~ 25 m upstream of the chamber in the probe beamline, which monitors backscatter from the seed laser pulse. This provides a trigger that can be synchronized with the time-of-flight of the laser by adjusting either the internal delay of the ICCD (≥ 45 ns) or the optical path length of the fibers (Figure 1(e)). The repeatability of this triggering mechanism reduces the necessary exposure time to capture the TS spectra (minimum gate 4 ns) and thereby maximizes the signal-to-noise ratio against the self-emission of the plasma, which is also integrated over the exposure window.

E. Signal processing and spectral fitting

The spectrometer ICCD records an image of the spatial extent of the slit (vertical axis) plotted against the spectrum of the light (horizontal axis) (Figure 2(a)). To extract the data, the ICCD image is split into horizontal bands representing each fiber. The number of pixel rows corresponding to each fiber is approximately 10 rows per 100 μm fiber diameter. Each row is treated as a separate measurement of the spectrum for that fiber, as this allows a weighted average of the spectrum to be calculated; this suppresses the statistical significance of any anomalous hot camera pixels prior to performing spectral fitting. In calculating the average spectrum, the rows are weighted by their integrated intensity across a fixed spectral range covering the width of the IAW feature (e.g. $\lambda_0 \pm 2$ Å). This therefore gives the greatest weighting to the rows at the center of the fiber, which are brightest.

Figures 2(b)-(d) show plots of the averaged IAW spectrum (blue dots) with $\pm 1\sigma$ (light blue shading) for several fibers in a single experiment. The spectra are fit with the nonrelativistic, Maxwellian spectral density function $S(K,\omega)$ (red dashed line), which is convolved with a Voigt profile
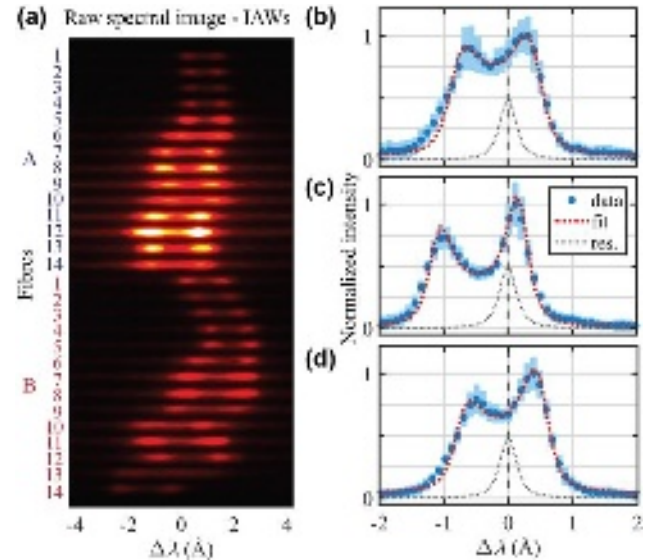

FIG. 2. (a) Raw ICCD image showing the IAWs of the TS spectra from two fiber arrays in a jet-interaction experiment[43]. (b-d) Examples of fitted IAW spectra from individual fibers in a magnetic reconnection experiment[22]. Grey line shows the instrument response of the spectrometer, scaled to 50% of the signal intensity.

characterizing the instrument response of the apparatus to the narrow laser line of the probe (grey line). This is recorded before the experiment by scattering the probe from the alignment needle. The fitting routine[35] uses a weighted least squares method, with additional free parameters for the stray laser light as well as a systematic offset in intensity to account for the combined contributions of the plasma self-emission (to good approximation uniform over the spectral range of the IAWs) and camera dark counts. As defined in Section IIA, the plasma parameters fit to the IAW TS spectra are: V_{flow} (determined from the central Doppler shift of the feature), T_i (width of the IAW peaks), $\bar{Z}T_e$ (separation of the peaks), n_e (shape of the IAWs via α-parameter) and U_{drift} (asymmetric height of the peaks). The product $\bar{Z}T_e$ is decomposed into self-consistent values using the non-local thermodynamic equilibrium (nLTE) model SpK[36]. Each of these variables can either be held fixed (such as n_e obtained from interferometry) or restricted by a lower bound. In cases where multiple spectra exist for the same spatial location in the plasma (i.e. multiple collection directions), the spectra can also be co-constrained with common fitting parameters (i.e. $n_e, T_i, \bar{Z}T_e$) to ensure consistency, as demonstrated in Refs. 19,25,26,37,38. In cases where the acceptance angle of the collection optics is large, an integral of $S(\boldsymbol{K}[\theta,\phi],\omega)$ needs to be calculated for the angular distribution of $\boldsymbol{K}$, in order to account for the broadening associated with the superposition of spectra[28].

III. EXPERIMENTAL RESULTS
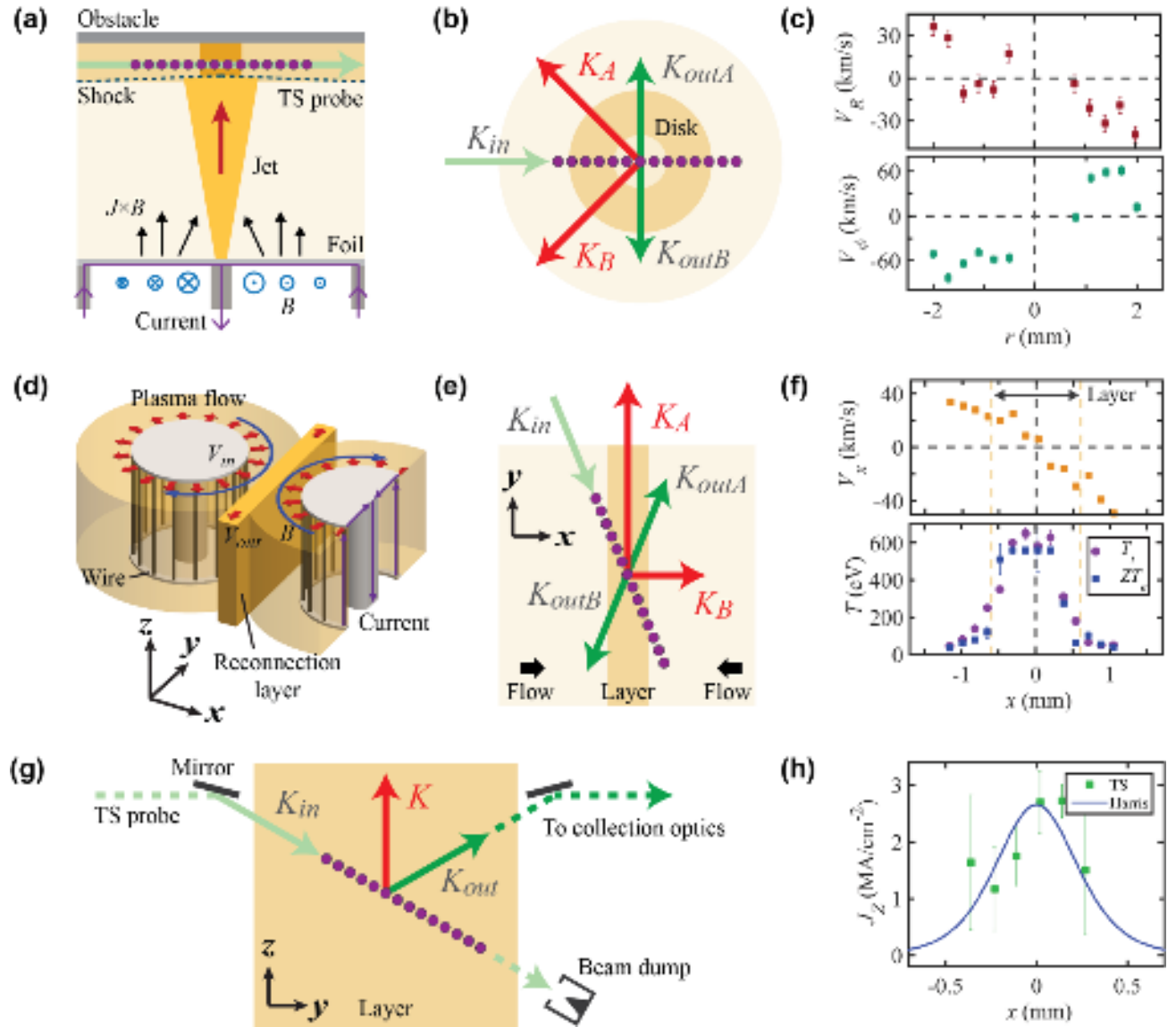
A. Flow velocity measurements in a 2D plane

FIG. 3. (a) Cross-sectional (side-on) schematic diagram of a jet-obstacle interaction experiment[43], with TS in the post-shock region. (b) TS geometry used to measure orthogonal velocity components in a rotating plasma disk[21,44]. (c) Radially and azimuthally resolved velocity components in a rotating plasma disk. (Reproduced from Ref. 44 with the permission of AIP Publishing.) (d) Schematic diagram of a magnetic reconnection layer formed between two exploding wire arrays[29]. (e) TS geometry used to make temperature and velocity measurements in the reconnection (xy) plane of (d). (f) Inflow velocity and temperature profiles of the reconnection layer from the TS geometry in (e). (Reproduced from Ref. 45 with the permission of AIP Publishing.) (g) TS geometry for electron drift velocity measurements in the reconnection layer, projected onto the xz-plane of the setup in (d). (h) Local measurements of the current density of the reconnection layer, overlaid with a Harris sheet profile calculated from Faraday rotation measurements of the integrated upstream magnetic field profile of the layer[46].

Figure 1(a) shows a top-down view of the TS probe beam propagating horizontally through experiment chamber. The deployment of two fiber arrays collecting scattered light from this probe path in different radial directions, allows simultaneous measurements of different velocity components confined to the horizontal plane (as demonstrated in Figure 1(b)). The combination of such measurements for matching scattering volumes allows the

construction of the full 2D velocity vector of the plasma flow (direction and magnitude) within the horizontal plane.

An example of TS data obtained in such a scattering geometry is shown in Figure 2(a). The experiment (illustrated by the side-on cross-sectional schematic in Figure 3(a)) consisted of a conical jet of plasma (produced by the ablation of a circular foil with radial current flow[39–42]) which collided with a planar obstacle to produce a reverse shock. The TS probe beam was directed horizontally through

the post-shock region, and scattered light was collected from volumes (represented by purple dots in Figure 3(a)) spanning the central region of the interaction. The two fiber arrays, designated A and B in Figure 2(a), collected light in the plane parallel to the shock, at 90° (into the page in Figure 3(a)) and 225° to the direction of the probe beam, respectively; resulting in scattering vectors at 135° and 202.5° to the probing direction. The large differences in the Doppler shifts of the IAWs of neighboring fibers on the CCD indicate steep velocity gradients along the path of the probe beam. The combined datasets of these fibers allowed the complex dynamics of the flows in the radial direction of post-shock region to be determined; identifying a contracting plasma column close to the axis of the jet, and a radial outflow of plasma in the surrounding region[43].

Another example of the use of paired observation directions to measure the 2D velocity distribution of a plasma structure was in experiments designed to study the rotational properties of a plasma disk formed inside a cylindrical wire array Z-pinch with a cusp magnetic field[21,44]. The disk was formed by merging streams of plasma, ablated from the wires with an off-axis trajectory of $\sim5°$. The disk was observed to maintain a hollow profile for a time period much longer than the hydrodynamic crossing timescale of the disk ($\Delta r / V_r$) indicating confinement to the outer part of the disk by the angular momentum of the plasma. To quantify the rotational profile of the disk, our TS diagnostic was implemented in the geometry shown in Figure 3(b). The TS probe beam passed along the diameter of the disk, and light was collected from opposite directions, orthogonal to the beam. This provided equal length scattering vectors, with orthogonal directions. Flow velocity measurements from each of these directions were combined to resolve the radial and angular velocity components of plasma flow in the disk. The profiles shown in Figure 3(c) demonstrate the radial inflow of plasma, coupled with the coherent angular motion of the plasma, which reverses symmetrically across the disk, confirming the disk's rotation.

B. Temperature measurements in magnetic reconnection experiments

Magnetic reconnection experiments performed on Magpie[22,23,45–47] have utilized TS to make detailed quantitative measurements of the in and out going energy fluxes of a reconnection current layer. The setup, shown in Figure 1(c) and illustrated schematically in Figure 3(d), consists of two side-by-side exploding wire arrays[48], which are driven in parallel to produce a collision between the cylindrically diverging magnetized plasma flows. The flows meet with oppositely directed embedded magnetic fields, leading to the formation of the reconnection layer in the mid-plane.

The experiments employed the TS geometry shown in Figure 3(e). The TS probe beam passed through the reconnection plane of the setup (xy-plane in Figure 3(d)), crossing the layer at an angle of 22.5°. TS light was observed

simultaneously from volumes both inside the layer and in the upstream regions on either side (at positions similar to those indicated on the interferogram of Figure 1(d)). The observation directions yielded orthogonal scattering vectors, sensitive to the x and y components of the plasma flow velocity. The results shown in Figure 3(f) plot the inflow velocity V_x and temperature parameters ($\bar{Z}T_e, T_i$) of the plasma against the x-coordinate of the flow. This shows that the initially supersonic inflows collide and stagnate inside the layer. Meanwhile, measurements of V_y show that once inside the layer the plasma picks up a significant outflow velocity directed along the length of the layer[23,45]. The temperature plots indicate the significant broadening of the TS spectra that was observed inside the layer. The initially cold upstream plasma ($T_i \approx \bar{Z}T_e \sim 50$ eV) is strongly heated inside the layer reaching ion and electron temperatures an order of magnitude greater. With these measurements of the plasma parameters, it was possible to compare the ingoing kinetic energy of the plasma with the thermal energy gained inside the layer[23,45]. From this we concluded that thermalization of the flow kinetic energy in the collision was not sufficient to account for these increases in temperature, and the remaining energy budget therefore had to be provided by the release of stored magnetic energy carried by the inflows.

C. Measurements of electron drift velocity in a reconnection current sheet

In addition to measuring bulk plasma flow velocities, TS has been used to measure the relative drift velocity between ions and electrons in the reconnection setup of Figure 3(d). The gradient of the magnetic field profile across the layer in the reconnection plane is expected to induce a current in the out-of-plane direction ($J_z = [1/\mu_0][\partial B_y/\partial x]$). To probe the drift velocities associated with this current, the TS geometry illustrated in Figure 3(g) provided a current-aligned scattering vector. The setup utilized a mirror inside the experiment chamber to deflect the TS probe beam through the layer at a trajectory of -30° to the horizontal. After passing through the layer, the transmitted fraction of the beam was deposited in a beam dump positioned below the setup, to prevent stray light from the impact of the beam with the base of the experiment chamber. Scattered light was observed from the plasma at an angle of +30°, by the means of a symmetrically placed mirror to direct the light to the collection optics at the chamber-side viewport. This provided a purely vertical scattering vector as indicated in Figure 3(g). Viewed as a projection onto the reconnection plane, the TS probe beam in these experiments was again orientated at 22.5° to the layer in this plane, providing simultaneous measurements from scattering volumes both in the layer and upstream regions, as demonstrated in Figure 1(d).

Figures 2(b)-(d) show the TS spectra recorded at the three most central scattering volumes inside the reconnection

layer. The spectra show a good signal-to-noise ratio, with the clearly defined ion-acoustic peaks of the IAW feature. In particular Figure 2(d) demonstrates that there is minimal stray laser light present in the data of this experiment: the small bulk Doppler shift of this spectrum places the ion-acoustic peaks either side of the initial laser wavelength, where there is a well-defined local minimum in the intensity profile that is accurately fit by $S(\mathbf{K},\omega)$ (red line). The asymmetries in the heights of the peaks in each spectrum indicates the magnitude and polarity of the local electron drift velocity in the direction of the scattering vector. In each case the height of the red-shifted peak is enhanced with respect to the blue-shifted peak. This signals electron flow in the -z direction, which is consistent with the expected current direction of the layer. Fits to the spectra at these locations yield drift velocities of the order of 100 km/s.

The drift velocity measurements can be combined with the interferometry data to calculate the current density inside the layer. The interferogram of the reconnection plane (Figure 1(d)) yields measurements of the line-integrated electron density $\int n_e dz$, which is divided by the vertical length of the arrays (Δz) to provide cross-sectional estimates of the local electron density. Figure 3(h) shows the calculated current density values ($J_z = e n_e U_{drift}$, green dots) at each of the scattering locations in the experiment. Away from the center of the layer the measurement uncertainties increase as the ion-acoustic peaks become harder to fit with the decreasing peak separation at lower values of $\bar{Z}T_e$. Beyond $|x|>0.4$ mm the peaks cannot be resolved, however the current density is expected to tend towards zero outside the reconnection layer.

It is interesting to compare these results with the current density profile inferred from independent measurements using our Faraday rotation polarimetry diagnostic[26]. This probed along the y-axis of the setup (Figure 3(d)) to record the line-integrated magnetic field distribution $\int n_e B_y dy$ of the plasma. This was divided by coaligned interferometry measurements of $\int n_e dy$ to estimate a field strength of $B_0 \sim 10$ T at the edges ($x = \pm \delta$) of the layer[46]. It can be assumed that the magnetic field distribution follows a Harris sheet profile across the layer $\left(B_y = B_0 \tanh[x/\delta] \rightarrow J_z = 1/\delta\mu_0 \operatorname{sech}^2[x/\delta]\right)$, which is overlaid on the plot of Figure 3(h) (blue line). The consistency between the independent measurements from TS and Faraday rotation should increase confidence in the use of TS data to infer local magnetic field profiles. This is a technique which has recently been used to interpret the results from a series of laser driven experiments on Weibel unstable plasmas[13,49].

IV. SUMMARY & FUTURE DEVELOPMENT

In this paper we have described a TS diagnostic used in pulsed-power driven HEDP experiments. The use of a fiber-optic based system allows scattered light to be collected from multiple spatially resolved locations in the plasmas and along different viewing directions simultaneously. It also offers flexibility to easily reconfigure the scattering

geometry between experiments to: (1) probe with scattering vectors that select the flow velocity components that are of most interest, (2) set the TS α-parameter to select the TS regime, and (3) maximize the spectral resolution through the magnitude of the K-vector.

To date, the diagnostic has been used to view the IAWs of the TS spectra, which are fit with the spectral density function $S(\mathbf{K},\omega)$ to extract measurements of the plasma parameters: $\left[n_e, T_i, \bar{Z}T_e, V_{flow}, U_{drift}\right]$. However, recent upgrades to the system include an additional imaging spectrometer (Andor Shamrock 500i, with Andor iStar 334T ICCD) to simultaneously observe the electron plasma waves (EPWs) of the TS spectra. The shape of this feature is dependent on the electron temperature[17], and so measurements of the IAWs and EPWs with common scattering volumes will allow both $\bar{Z}$ and T_e to be determined without the need to rely on models to separate the product $\bar{Z}T_e$. To view the broader EPW spectral feature (typically several nanometers wide) the spectrometer is equipped with a range of gratings, including a 1200 lines/mm grating, which in combination with the 1024×1024-pixel ICCD provides a spectral range of $\lambda_0 \pm 10$ nm. To accommodate the lower signal intensity of the EPW feature a slit width of 100 μm maximizes the accepted light, resulting in a resolution of 2Å. The system has been successfully implemented on experiments diagnosing the outflow from a plasma gun[28], where the EPWs were observed both in the collective ($\alpha>1$) and non-collective ($\alpha<1$) regimes. Experiments on Magpie are planned to follow shortly, however this will introduce the additional challenge of detecting the EPWs above the intense self-emission of the high atomic number, HEDP plasmas.

The addition of a second spectrometer will also allow data to be taken at an increased number of time intervals throughout the 8 ns window of the probe laser pulse. This can be achieved either by triggering the spectrometers with separate programmed delays with respect to the trigger diode, or by introducing separate time-of-flight delays to the scattered light by varying the path lengths of the individual optical fibers (Figure 1(e)). The ICCD accompanying the second spectrometer has a reduced minimum gate time of ≥ 2 ns, allowing several unique time intervals to be sampled throughout the pulse duration.
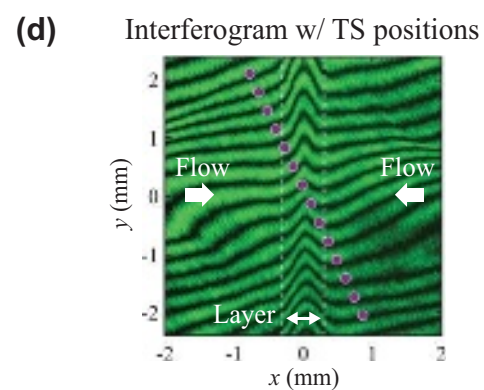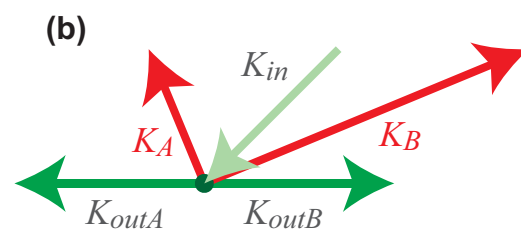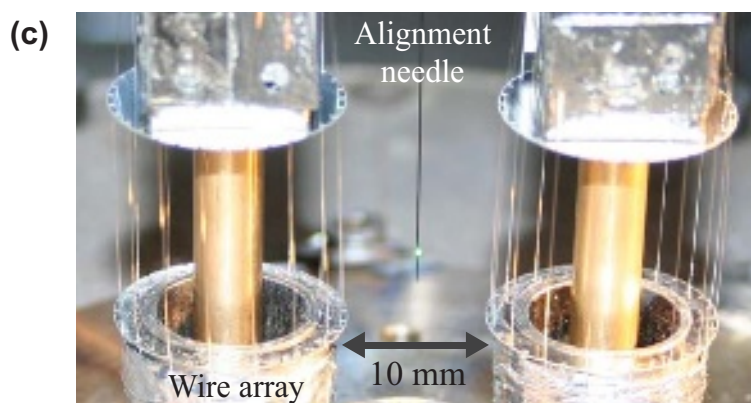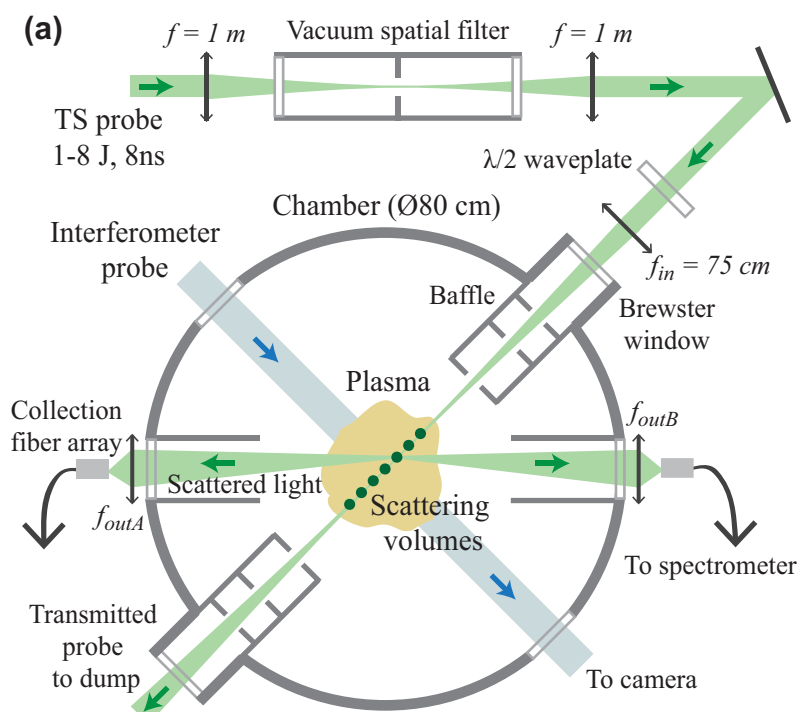
DATA AVAILABILITY

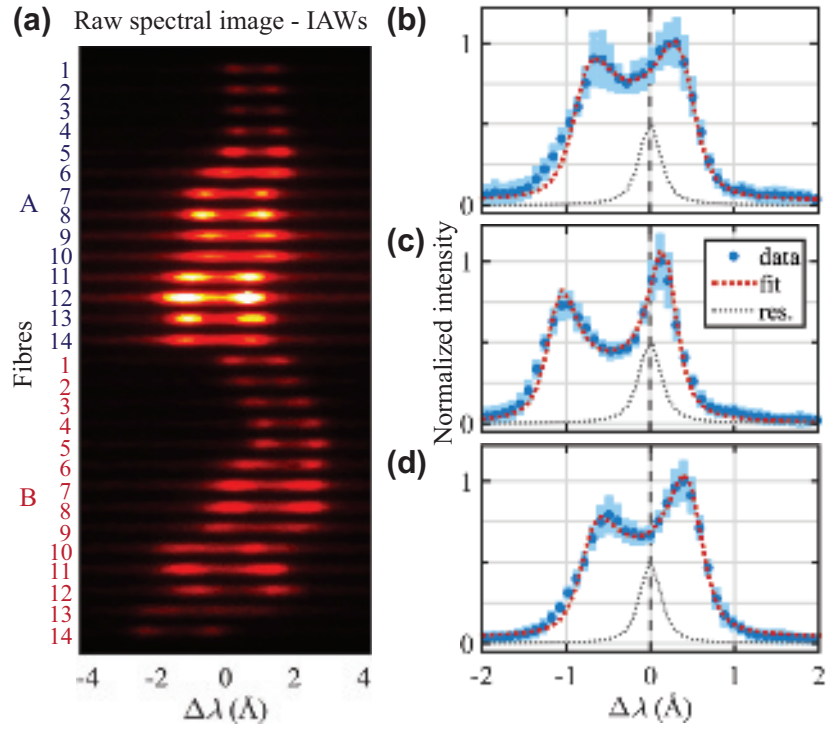The data that support the findings of this study are available from the corresponding author upon reasonable request.

[1] I.H. Mitchell *et al.*, Rev. Sci. Instrum. **67**, 1533 (1996).

[2] L.G. Suttle *et al.*, Plasma Phys. Control. Fusion **62**, 014020 (2020).

[3] S. V. Lebedev, A. Frank, and D.D. Ryutov, Rev. Mod. Phys. **91**, 025002 (2019).

[4] S.H. Glenzer *et al.*, Phys. Rev. Lett. **86**, 2565 (2001).

[5] A.J. Mackinnon *et al.*, Rev. Sci. Instrum. **75**, 3906 (2004).

[6] D.H. Froula *et al.*, Rev. Sci. Instrum. **77**, 10E522 (2006).

[7] J.S. Ross *et al.*, Rev. Sci. Instrum. **77**, 10E520 (2006).

[8] J.S. Ross *et al.*, Rev. Sci. Instrum. **81**, 10D523 (2010).

[9] T. Gong *et al.*, Rev. Sci. Instrum. **86**, 023501 (2015).

[10] P.S. Datte *et al.*, Rev. Sci. Instrum. **87**, 11E549 (2016).

[11] S.V.R. Rocco *et al.*, Rev. Sci. Instrum. **89**, 10C117 (2018).

[12] J.T. Banasek *et al.*, Rev. Sci. Instrum. **89**, 10C109 (2018).

[13] G.F. Swadling *et al.*, Phys. Rev. Lett. **124**, 215001 (2020).

[14] D.S. Montgomery, J.L. Kline, and T.E. Tierney, Rev. Sci. Instrum. **75**, 3793 (2004).

[15] A.M. Hansen *et al.*, Rev. Sci. Instrum. **89**, 10C103 (2018).

[16] S. Le Pape *et al.*, Phys. Rev. Lett. **124**, 025003 (2020).

[17] D.H. Froula, S.H. Glenzer, N.C.J. Luhmann, and J. Sheffield, *Plasma Scattering of Electromagnetic Radiation*, 2nd Ed. (Elsevier, 2011).

[18] A.J. Harvey-Thompson *et al.*, Phys. Rev. Lett. **108**, 145002 (2012).

[19] G.F. Swadling *et al.*, Phys. Rev. Lett. **113**, 035003 (2014).

[20] S. V. Lebedev *et al.*, Phys. Plasmas **21**, 056305 (2014).

[21] M.J. Bennett *et al.*, High Energy Density Phys. **17**, 63 (2015).

[22] L.G. Suttle *et al.*, Phys. Rev. Lett. **116**, 225001 (2016).

[23] J.D. Hare *et al.*, Phys. Rev. Lett. **118**, 085001 (2017).

[24] G.C. Burdiak *et al.*, Phys. Plasmas **24**, 072713 (2017).

[25] Y. Liu, Y. Ding, and J. Zheng, Rev. Sci. Instrum. **90**, 083501 (2019).

[26] G.F. Swadling *et al.*, Rev. Sci. Instrum. **85**, 11E502 (2014).

[27] G.F. Swadling *et al.*, Phys. Plasmas **20**, 022705 (2013).

[28] J.D. Hare *et al.*, Plasma Phys. Control. Fusion **61**, 085012 (2019).

[29] A.J. Harvey-Thompson *et al.*, Phys. Plasmas **19**, 056303 (2012).

[30] J. Dawson and C. Oberman, Phys. Fluids **5**, 517 (1962).

[31] J.M. Dawson, Phys. Fluids **7**, 981 (1964).

[32] T.W. Johnston and J.M. Dawson, Phys. Fluids **16**, 722 (1973).

[33] S. Pfalzner and P. Gibbon, Phys. Rev. E **57**, 4698 (1998).

[34] A.E. Siegman, *Lasers* (University Science Books, 1986).

[35] J.D. Hare, *High Energy Density Magnetic Reconnection Experiments in Colliding Carbon Plasma Flows*, Imperial College London, 2017.

[36] N.-P.L. Niasse, *Development of a Pseudo Non-LTE Model for Z-Pinch Simulations*, Imperial College London, 2011.

[37] G.F. Swadling *et al.*, Phys. Plasmas **22**, 072706 (2015).

[38] G.F. Swadling *et al.*, Phys. Plasmas **23**, 056309 (2016).

[39] F. Suzuki-Vidal *et al.*, Astrophys. Space Sci. **322**, 19 (2009).

[40] F. Suzuki-Vidal *et al.*, Phys. Plasmas **17**, 112708 (2010).

[41] S. V. Lebedev *et al.*, Proc. Int. Astron. Union **6**, 26 (2010).

[42] F. Suzuki-Vidal *et al.*, Astrophys. Space Sci. **336**, 41 (2011).

[43] E.R. Tubman *et al.*, in *61st Annu. Meet. APS Div. Plasma Phys.* (Fort Lauderdale, Florida, 2019).

[44] M.J. Bennett *et al.*, AIP Conf. Proc. **1639**, 71 (2014).

[45] J.D. Hare *et al.*, Phys. Plasmas **24**, 102703 (2017).

[46] L.G. Suttle *et al.*, Phys. Plasmas **25**, 042108 (2018).

[47] J.D. Hare *et al.*, Phys. Plasmas **25**, 055703 (2018).

[48] A.J. Harvey-Thompson *et al.*, Phys. Plasmas **16**, 022701 (2009).

[49] C. Bruulsema *et al.*, Phys. Plasmas **27**, 052104 (2020).

(a) f = 1 m   Vacuum spatial filter   f = 1 m

TS probe
1-8 J, 8ns

λ/2 waveplate

f_{in} = 75 cm

Interferometer
probe

Chamber (Ø80 cm)

Baffle

Brewster
window

Plasma

Collection
fiber array

f_{outB}

Scattered light

f_{outA}

Scattering
volumes

To spectrometer

Transmitted
probe
to dump

To camera

(b)

K_{in}

K_A K_B

K_{outA} K_{outB}

(d) Interferogram w/ TS positions

Flow   Flow

Layer

y (mm)

x (mm)

(c) Alignment
needle

Wire array   10 mm

(e) Focusing
telescope   Spectrometer

Slit

Length 2-4 m

Grating

ICCD

A   B

Collection
fiber arrays

Trigger diode

(a) Raw spectral image - IAWs

(a) Obstacle, Shock, TS probe, Jet, J×B, Foil, Current, B

(b) K_A, K_{outA}, K_{in}, Disk, K_B, K_{outB}

(c) V_R (km/s), V_ϕ (km/s), r (mm)

(d) Plasma flow, V_{in}, V_{out}, B, Wire, Current, Reconnection layer, z, y, x

(e) K_{in}, K_A, K_{outA}, y, x, K_{outB}, K_B, Flow, Layer, Flow

(f) V_x (km/s), Layer, T (eV), T_i, ZT_e, x (mm)

(g) Mirror, K_{in}, K, To collection optics, TS probe, K_{out}, z, y, Layer, Beam dump

(h) J_Z (MA/cm^{-2}), TS, Harris, x (mm)